J. Fluid Mech. (1978), *vol.* 86, *part* 4, *pp.* 761–781
Printed in Great Britain

A depth-averaged mathematical model for the near field of side discharges into open-channel flow

By J. J. McGUIRK AND W. RODI
Sonderforschungsbereich 80, University of Karlsruhe, Germany

(Received 26 October 1977)

A two-dimensional mathematical model is described for the calculation of the depth-averaged velocity and temperature or concentration distribution in open-channel flows, an essential feature of the model being its ability to handle recirculation zones. The model employs the depth-averaged continuity, momentum and temperature/concentration equations, which are solved by an efficient finite-difference procedure. The 'rigid lid' approximation is used to treat the free surface. The turbulent stresses and heat or concentration fluxes are determined from a depth-averaged version of the so-called k, ϵ turbulence model which characterizes the local state of turbulence by the turbulence kinetic energy k and the rate of its dissipation ϵ. Differential transport equations are solved for k and ϵ to determine these two quantities. The bottom shear stress and turbulence production are accounted for by source/sink terms in the relevant equations. The model is applied to the problem of a side discharge into open-channel flow, where a recirculation zone develops downstream of the discharge. Predicted size of the recirculation zone, jet trajectories, dilution, and isotherms are compared with experiments for a wide range of discharge to channel velocity ratios; the agreement is generally good. An assessment of the numerical accuracy shows that the predictions are not influenced significantly by numerical diffusion.

1. Introduction

1.1. *Problem considered*

The most common form of waste disposal into rivers is, for reasons of constructional economy, the side discharge over the full water depth, a configuration which has been used for the rejection of both waste water and waste heat. The present paper is concerned with the development of a method for predicting the velocity and pollutant-concentration fields induced by such discharges. A typical flow situation is illustrated in figure 1 (*a*) for the case of a discharge at right-angles to the river direction; attention is restricted to this case in the present paper. The discharge jet is deflected by the river cross-flow, at the same time forcing the river flow to bend towards the far bank. The jet entrainment on the near-bank side is restricted by the presence of the solid boundary, causing a recirculation region with low pressure (decreased surface elevation) to form behind the jet. Owing to this low pressure, the jet bends towards the near bank and eventually attaches itself to the wall. The occurrence of a recirculation region is a characteristic feature of full-depth side discharges and considerably complicates the mathematical solution of this problem.

The size of the recirculation zone is governed mainly by the ratio of discharge to river momentum. The parameters determining this ratio are, for rectangular river and

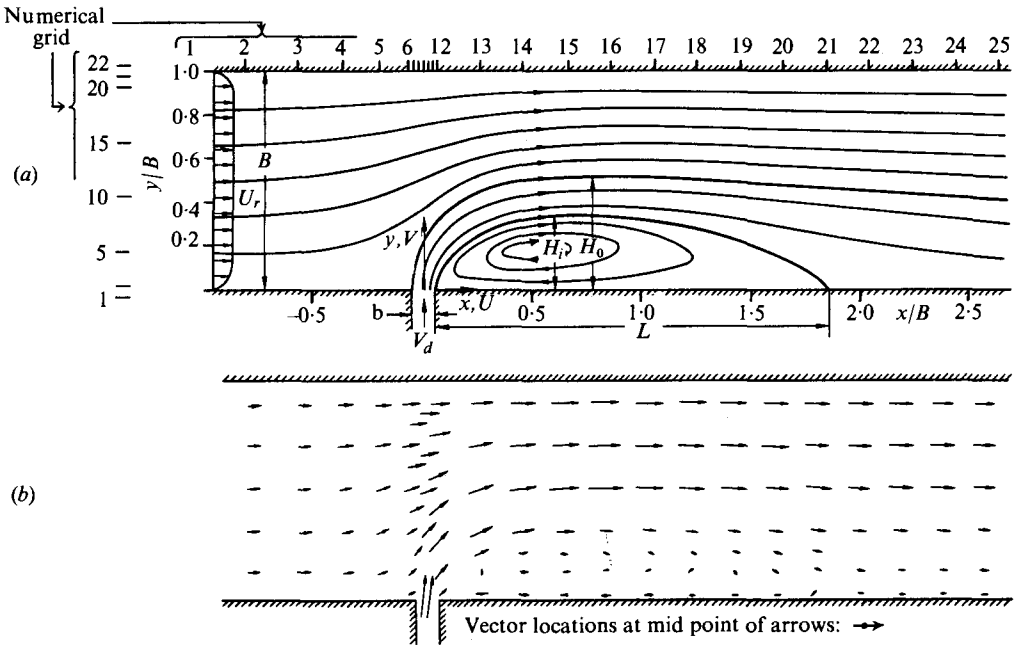

FIGURE 1. (a) Flow configuration and streamline pattern; (b) velocity vectors.

jet cross-sections as assumed in this study, the river and discharge widths B and b, and the corresponding average velocities U_r and V_d. The flow is further influenced by the presence of the river bottom, which exerts a shear stress and causes additional turbulence production. The parameters governing this influence are the water depth h and the bed roughness. Buoyancy effects, which may lead to stratification of the flow, are considered negligible for the discharges treated in this paper; for this reason, and because the discharge extends over the full depth of the river and is uniform, the flow quantities will vary little with depth, so that only their horizontal variation is of interest.

The distribution of pollutant concentration, such as the temperature rise due to cooling water discharge from power stations, is of great concern to environmentalists, who must assess possible detrimental effects on the ecology of the river. For rivers which are navigable and which carry appreciable ship and barge traffic, the potentially hazardous cross-river velocities induced by large discharges form an additional point of interest. It is therefore important to be able, at the planning stage, to predict both velocity and pollutant fields caused by an intended discharge.

The development of mathematical models for the region far downstream of the discharge where the velocity field has returned to its 'normal' state (i.e. the disturbances due to the discharge have all but disappeared) has received considerable attention (Jirka, Abraham & Harleman 1975). However, all far-field models are dependent on accurate input of the starting profiles, which are governed by the near-field behaviour. In addition, regulatory requirements specify conditions which are most likely to be violated in the area close to the discharge. Both these facts indicate the importance of near-field mathematical models, which, unfortunately, are in a less well-tested stage of development, in particular for the flow situation of interest here.

Consequently recourse is usually made to laboratory modelling; one-off hydraulic models are built to study each planned design or to deliver the starting profiles required by the far-field models. The model presented here was developed to avoid this time- and money-consuming process.

1.2. *Previous work*

One of the first investigations of a flow related to the side discharge problem was the detailed wind-tunnel measurements of Rouse (1957) in a plane two-dimensional jet in effectively unconfined cross-flow. From his data Rouse found that the length of the recirculation zone (L in figure 1), non-dimensionalized with the discharge width b, increases with the $\frac{3}{2}$ power of the velocity ratio V_d/U_r.

This geometry and ones like it have also been studied theoretically and experimentally many times since, mainly owing to its application as one method of turbine blade cooling. Although much can be learned about the present problem from these studies, two important phenomena, which are peculiar to the side discharge situation, are missing: the influence of the far bank, and the influence of the river bottom. Accordingly, only work of direct relevance to the side discharge problem has been used in the development and testing of the model, although unfortunately this is much less abundant.

Mikhail, Chu & Savage (1975) have measured the width and length of the recirculation eddy in the open-channel flow situation described above. From dimensional analysis they concluded that the shape of the eddy is unaffected by the width ratio b/B and that the size of the eddy depends mainly on the momentum flux ratio $M = V_d^2 b/U_r^2 B$; their measurements confirmed this analysis at least for small values of b/B. Carter (1969) measured the temperature field set up by a warm water discharge into a flume and studied the influence of the velocity ratio $R = V_d/U_r$ including at least one case where the far wall of the channel influenced the jet spreading. Strazisar & Prahl (1973) evaluated the jet trajectory from dye photographs and examined the influence of the velocity ratio R, the jet Reynolds number, the jet depth to width ratio h/b, and the channel to jet width ratio B/b. The Reynolds number had little effect while the maximum jet penetration (made dimensionless with b) increased with increasing R, h/b, and B/b; the latter influence was however of importance only for the larger velocity ratios.

A brief review of existing theoretical models for the side discharge problem will now be given. Mikhail *et al.* (1975) used a global control-volume analysis to obtain a relation between the recirculation-eddy size and the momentum-flux ratio; adjustment of the single empirical constant involved yielded fair agreement with their experiments. Carter (1969) developed a rather crude momentum-integral type method to predict the jet trajectory, but only to the point of maximum penetration. The method is based on the assumption of 'top-hat' profiles and requires the dilution rate as empirical input; this Carter obtained from his own experiments; effects of the far bank and bottom are not included. Apart from the limited information obtainable from the method, some of the assumptions involved are rather questionable, as was discussed in detail by Policastro & Tokar (1972). In particular, the evaluation of the drag force on the jet via the introduction of a constant empirical drag coefficient C_D led to appreciable underprediction of the jet trajectory at large values of R. Strazisar & Prahl (1973) have extended Carter's method to include the effect of bottom friction, but found that they still had to adjust the value of C_D to obtain agreement at various velocity ratios.

The theoretical models discussed so far were developed for and are restricted to the side discharge problem. More general models employing the governing partial differential equations are also available and can, in principle, be applied to this problem. Leendertse (1967) proposed a two-dimensional depth-averaged model for unsteady free-surface flows which has been used by Kuipers & Vreugdenhil (1973) to predict steady recirculating flows in harbours and bays. The model neglects the turbulent transport terms in the equations, but, owing to a smoothing procedure introduced to obtain numerical stability in their central difference scheme, terms which exert a diffusive action are effectively introduced. This is physically unreasonable, since the diffusion present in the numerical solution then depends only on the smoothing coefficient used. Since turbulent transport processes are very important in jet-type flows, this model is not suitable for the near field of the side discharge problem. A depth-averaged finite element method was applied to a thermal discharge problem by Loziuk, Anderson & Belytschko (1972). The velocity field was obtained from potential flow calculations with superposition of the jet flow as extracted from experiments, the turbulent diffusion coefficient in the temperature equation was assumed constant over the whole domain and was also determined from experiments. Because this method contains very little physical input of general validity, its range of applicability is certainly very limited.

From this short review, one may conclude that the existing simple control-volume and integral methods cannot provide the whole velocity and pollutant concentration fields but only a few features of them; while the numerical models, which could in principle give this detailed information, use highly inadequate descriptions of the turbulence processes.

1.3. *Present contribution*

In the fields of mechanical and aeronautical engineering, mathematical models have been developed for two-dimensional recirculating flows which employ advanced turbulence models. These calculation procedures have been applied successfully in areas which have much in common with the present flow situation, e.g. film cooling, jet ejectors and many other problems (see e.g. Launder & Spalding 1974), and the turbulence models have been tested extensively for jet flows (Launder *et al.* 1972). Therefore, these models appear sufficiently refined to promise success for the open-channel discharge problem. The calculation procedures were, however, developed for strictly two-dimensional flows and thus are not directly applicable to open-channel flows where bottom and surface effects may be important. It is the purpose of this paper to describe an extension of these procedures to yield a depth-averaged mathematical model for open-channel flows, and to report on extensive testing of this model by comparison with laboratory experiments.

The model employs the depth-averaged forms of the continuity, momentum and temperature or concentration equations, with terms arising from non-uniform vertical distributions neglected so that buoyancy effects cannot be accounted for; these equations are introduced in § 2.1. The next section describes the turbulence model used in calculating the turbulent viscosity and diffusivities, and the way in which the turbulence generation due to bottom shear is accounted for in this model. Section 2.3 presents details on the numerical solution procedures and the boundary conditions employed. Results of the model applied to the side discharge problem illustrated in figure 1 are presented, discussed and compared with experiments in § 3. A discussion of the

important physical processes governing the development of the flow in various areas of the near field is also given as this throws light on the numerical accuracy of the calculations from the point of view of 'false' diffusion; some input sensitivity tests are also reported. The final section will draw conclusions on the performance and the range of applicability of the present model.

2. Mathematical model

Open-channel flow is always strictly three-dimensional; however, this feature is often of secondary importance, especially when the width to depth ratio is large and the channel bed is rough so that strong vertical mixing leads to a nearly-uniform vertical distribution of the flow quantities. Therefore, a two-dimensional description of the flow is sufficient in many cases. The mathematical model described below makes use of this special feature; it is a two-dimensional model for calculating the horizontal distribution of the depth-averaged velocity components $\bar{U}$ and $\bar{V}$, the local water depth h, and a depth-averaged scalar quantity $\bar{\Phi}$. These depth-averaged quantities are defined by the following relations:

$$\bar{U} = \frac{1}{h}\int_{z_B}^{z_B+h} U\,dz, \quad \bar{V} = \frac{1}{h}\int_{z_B}^{z_B+h} V\,dz, \quad \bar{\Phi} = \frac{1}{h}\int_{z_B}^{z_B+h} \Phi\,dz, \tag{1}$$

where z is the vertical co-ordinate and z_B represents the channel bottom. In the present paper Φ may stand for temperature or species concentration, but will be referred to as temperature only in the remainder of the paper. In the present problem the velocity field is independent of the Φ distribution, but of course the opposite is not the case. Attention is restricted here to steady flow situations.

2.1. *Mean flow equations*

Equations governing the distribution of $\bar{U}$, $\bar{V}$ and h can be obtained by integrating the three-dimensional continuity and momentum equations over the water depth. The details of the integration may be found in Kuipers & Vreugdenhil (1973). With the simplifications discussed below, the results are as follows (the co-ordinate system is shown in figure 1*a*):

$$\frac{\partial \bar{U}}{\partial x} + \frac{\partial \bar{V}}{\partial y} = 0, \tag{2}$$

$$\frac{\partial \bar{U}^2}{\partial x} + \frac{\partial \bar{V}\bar{U}}{\partial y} = \frac{\partial}{\partial x}\left(\frac{\bar{\tau}_{xx}}{\rho}\right) + \frac{\partial}{\partial y}\left(\frac{\bar{\tau}_{xy}}{\rho}\right) - g\frac{\partial h}{\partial x} - \frac{\tau_{bx}}{\rho h}, \tag{3}$$

$$\frac{\partial \bar{U}\bar{V}}{\partial x} + \frac{\partial \bar{V}^2}{\partial y} = \frac{\partial}{\partial x}\left(\frac{\bar{\tau}_{xy}}{\rho}\right) + \frac{\partial}{\partial y}\left(\frac{\bar{\tau}_{yy}}{\rho}\right) - g\frac{\partial h}{\partial y} - \frac{\tau_{by}}{\rho h}. \tag{4}$$

Similarly, an equation governing the distribution of $\bar{\Phi}$ may be obtained by integration of the three-dimensional transport equation for Φ:

$$\frac{\partial \bar{U}\bar{\Phi}}{\partial x} + \frac{\partial \bar{V}\bar{\Phi}}{\partial y} = \frac{\partial}{\partial x}\left(\frac{\bar{J}_{\phi x}}{\rho}\right) + \frac{\partial}{\partial y}\left(\frac{\bar{J}_{\phi y}}{\rho}\right). \tag{5}$$

In the momentum equations (3) and (4), the pressure gradients have been replaced by the gradients of water depth h via the hydrostatic pressure assumption (g is gravitational acceleration). The present model is restricted to flow in rectangular channels

with horizontal bottoms where gradients of water depth and surface elevation (defined above some horizontal datum) are identical; in general situations the latter enter the momentum equations.† The variation of water depth was neglected above in the continuity equation (2) and in the diffusion terms of (3)–(5). This neglect is known as the rigid lid approximation and is valid when the water depth variations are small compared with the water depth itself, as can be seen from the exact depth-averaged continuity equation as used by Kuipers & Vreugdenhil (1973):

$$\frac{\partial \overline{U}h}{\partial x}+\frac{\partial \overline{V}h}{\partial y}=\frac{\partial \overline{U}}{\partial x}+\frac{\partial \overline{V}}{\partial y}+\frac{\overline{U}}{h}\frac{\partial h}{\partial x}+\frac{\overline{V}}{h}\frac{\partial h}{\partial y}=0.$$

Owing to the use of the rigid lid approximation, the present model cannot be applied to long stretches of gradually varied flow where the water depth can vary significantly in the streamwise direction. However, such application is in any case not advisable or intended since the model is particularly suited to the (usually short) stretches with recirculation zones; for long stretches without recirculation zones a simpler and more economic boundary-layer type model is available (Rastogi & Rodi 1978) which can take full account of the streamwise variation of h.

τ_{bx} and τ_{by} are the bottom shear stresses in the x and y direction respectively (wind shear stresses at the surface are neglected). They are calculated by relating them to the depth-averaged velocities via:

$$\frac{\tau_{bx}}{\rho}=c_f\,\overline{U}(\overline{U}^2+\overline{V}^2)^{\frac{1}{2}},\quad \frac{\tau_{by}}{\rho}=c_f\,\overline{V}(\overline{U}^2+\overline{V}^2)^{\frac{1}{2}}, \tag{6}$$

where c_f is an empirical friction factor, for which the value $c_f = 0{\cdot}003$ is adopted in this paper (a mean value taken from Spalding (1975) corresponding to smooth channels).

Equations (3)–(5) as described by Kuipers & Vreugdenhill (1973) contained further terms accounting for vertical non-uniformity of the $\overline{U}$, $\overline{V}$, and $\overline{\Phi}$ profiles. In the case of the $\overline{\Phi}$ equation for example the extra terms are:

$$A_\phi=-\frac{\partial I_{u\phi}}{\partial x}-\frac{\partial I_{v\phi}}{\partial y},$$

where $$I_{u\phi}=\frac{1}{h}\int_{z_B}^{z_B+h}(U-\overline{U})(\Phi-\overline{\Phi})\,dz,\quad I_{v\phi}=\frac{1}{h}\int_{z_B}^{z_B+h}(V-\overline{V})(\Phi-\overline{\Phi})\,dz.$$

The A_ϕ terms arise from splitting local quantities Φ into depth-averaged values $\overline{\Phi}$ and deviations $(\Phi-\overline{\Phi})$ and then carrying out the depth-averaging of the equations; this is in direct analogy with the occurrence of the Reynolds stresses when the Navier–Stokes equations are time-averaged for turbulent flows. The physical meaning of the resulting terms is also equivalent: the integrals I defined above are depth-averaged $\overline{\Phi}$ fluxes. This transport of depth-averaged quantities due to vertical non-uniformities is usually called dispersion in the literature (see Fischer 1973). In the present model these terms are neglected on the assumption that the vertical profiles are nearly uniform in the channel flows considered here. Rastogi & Rodi (1978) have calculated these dispersion terms with the aid of a three-dimensional model and have found that they are negligible

† This is easily incorporated by replacing $g(\partial h/\partial x)$ by $g[(\partial z_B/\partial x)+\partial h/\partial x]$ with a corresponding change to $g(\partial h/\partial y)$; $z_B(x, y)$ is the (known) bottom topography.

in the boundary-layer type flow considered by them. Only comparison of model predictions with experiments can show whether the neglect is also justified in the side discharge problem involving recirculation zones.

2.2. *Turbulence model*

The momentum equations (3) and (4) contain the depth-averaged turbulent stresses $\bar{\tau}_{xx}$, $\bar{\tau}_{yy}$ and $\bar{\tau}_{xy}$, and the temperature equation (5) the depth-averaged turbulent heat fluxes $\bar{J}_{\phi x}$ and $\bar{J}_{\phi y}$. A turbulence model is needed to determine the horizontal distribution of these stresses and fluxes over the flow domain.

As was mentioned in § 1, advanced turbulence models have been used successfully to predict a variety of two-dimensional flows, including several with recirculation zones, but excluding open-channel flows. The model that found widest application and was tested most extensively is the so-called k, ϵ turbulence model which characterizes the local state of turbulence by two parameters: the turbulent kinetic energy k and the rate of its dissipation ϵ. A detailed description of this model and its applications was given by Launder & Spalding (1974).

Rastogi & Rodi (1978) have adapted the model for use in open-channel flow calculations, and their version is employed here. In analogy with the original k, ϵ model they assumed that the local depth-averaged state of turbulence can be characterized by the turbulence energy and dissipation parameters $\tilde{k}$ and $\tilde{\epsilon}$ and that the depth-averaged turbulent stresses and heat fluxes can be calculated from these parameters by means of the following relations (using tensor notation for simplicity):

$$\frac{\bar{\tau}_{ij}}{\rho} = \tilde{\nu}_t \left(\frac{\partial \bar{U}_i}{\partial x_j} + \frac{\partial \bar{U}_j}{\partial x_i} \right) - \tfrac{2}{3} \tilde{k} \delta_{ij}, \quad \frac{\bar{J}_{\phi i}}{\rho} = \tilde{\Gamma}_\phi \frac{\partial \bar{\Phi}}{\partial x_i}, \tag{7}$$

with

$$\tilde{\nu}_t = c_\mu \frac{\tilde{k}^2}{\tilde{\epsilon}}, \quad \tilde{\Gamma}_\phi = \frac{\tilde{\nu}_t}{\sigma_\phi}, \tag{8}$$

where c_μ and σ_ϕ are empirical constants and δ_{ij} is the Kronecker delta. Equation (7) introduces the turbulent viscosity/diffusivity concept and (8) presents a model for calculating the turbulent viscosity $\tilde{\nu}_t$ and the diffusivity $\tilde{\Gamma}_\phi$. These parameters, as well as $\tilde{k}$ and $\tilde{\epsilon}$, cannot be considered true depth-average quantities in the sense of the mathematical definition of (1); rather (7) defines the turbulent viscosity and diffusivity such that, when they are multiplied by the relevant gradient of the transported property, the depth-averaged turbulent shear stress or heat flux is obtained. The variation of $\tilde{k}$ and $\tilde{\epsilon}$ is determined from the following transport equations:

$$\frac{\partial \bar{U}\tilde{k}}{\partial x} + \frac{\partial \bar{V}\tilde{k}}{\partial y} = \frac{\partial}{\partial x}\left(\frac{\tilde{\nu}_t}{\sigma_k} \frac{\partial \tilde{k}}{\partial x} \right) + \frac{\partial}{\partial y}\left(\frac{\tilde{\nu}_t}{\sigma_k} \frac{\partial \tilde{k}}{\partial y} \right) + G + P_{kv} - \tilde{\epsilon}, \tag{9}$$

$$\frac{\partial \bar{U}\tilde{\epsilon}}{\partial x} + \frac{\partial \bar{V}\tilde{\epsilon}}{\partial y} = \frac{\partial}{\partial x}\left(\frac{\tilde{\nu}_t}{\sigma_\epsilon} \frac{\partial \tilde{\epsilon}}{\partial x} \right) + \frac{\partial}{\partial y}\left(\frac{\tilde{\nu}_t}{\sigma_\epsilon} \frac{\partial \tilde{\epsilon}}{\partial y} \right) + c_1 \frac{\tilde{\epsilon}}{\tilde{k}} G + P_{\epsilon v} - c_2 \frac{\tilde{\epsilon}^2}{\tilde{k}}, \tag{10}$$

where

$$G = \tilde{\nu}_t \left[2\left(\frac{\partial \bar{U}}{\partial x} \right)^2 + 2\left(\frac{\partial \bar{V}}{\partial y} \right)^2 + \left(\frac{\partial \bar{U}}{\partial y} + \frac{\partial \bar{V}}{\partial x} \right)^2 \right] \tag{11}$$

is the production of turbulent kinetic energy due to interactions of turbulent stresses with horizontal mean velocity gradients, and c_1, c_2, σ_k and σ_ϵ are further empirical constants. Equations (9) and (10) can be considered as depth-averaged forms of the

c_μ	c_1	c_2	σ_k	σ_ϵ	σ_ϕ
0·09	1·43	1·92	1·0	1·3	0·9

TABLE 1. Empirical constants in turbulence model.

three-dimensional k and ϵ equations (presented by Launder & Spalding 1974) when all terms originating from non-uniformity of vertical profiles are assumed to be absorbed in the source terms P_{kv} and $P_{\epsilon v}$. The main contribution to these terms stems from significant vertical velocity gradients near the bottom which, by interaction with the relatively large turbulent shear stresses in this region, produce turbulence energy. This production is in addition to the production G due to horizontal velocity gradients and depends strongly on the bottom roughness. Because it is governed by the near-bottom region, Rastogi & Rodi (1978) related these additional vertical production terms to the bottom shear stress τ_b via the friction velocity U_*, with the following result:

$$P_{kv} = c_k \frac{U_*^3}{h}, \quad P_{\epsilon v} = c_\epsilon \frac{U_*^4}{h^2}, \tag{12}$$

where $U_* = [c_f(\overline{U}^2 + \overline{V}^2)]^{\frac{1}{2}}$. They determined the empirical constants c_k and c_ϵ from undisturbed normal channel flow with Laufer's† (1951) measured turbulent viscosity as empirical input; they thus obtained:

$$c_k = \frac{1}{\sqrt{c_f}}, \quad c_\epsilon = 3{\cdot}6 \frac{c_2}{c_f^{\frac{3}{4}}} \sqrt{c_\mu}. \tag{13}$$

A value for the friction coefficient c_f was given above; the values for the remaining empirical constants in the turbulence model were simply adopted from Launder & Spalding (1974) and are given in table 1.

The practical significance of including the additional production terms P_{kv} and $P_{\epsilon v}$ as defined above is to ensure that the level of $\tilde{\nu}_t$ does not fall below that value pertaining to normal channel flow.

2.3. *Solution algorithm and computional details*

The above equation set has been solved numerically using the solution algorithm of Patankar & Spalding (1972) as incorporated in a computer program for two-dimensional elliptic flows by Gosman & Pun (1973). The differential equations are reduced to algebraic ones by integration over control volumes surrounding each grid node using assumptions for the variation of the variables between grid nodes. The main problem in solving the resultant set of algebraic equations lies in the determination of the pressure field (in the present case the local water depth h). Patankar & Spalding (1972) proposed a guess-and-correct procedure whereby a guessed pressure field is used to evaluate the velocity field, which, however, will not necessarily satisfy the continuity equation. By successive corrections to the pressure field the velocities are found which satisfy both the momentum and continuity equations. This process necessitates iterative solution of the algebraic equations. The measure of convergence used was

† Nakagawa *et al.* (1975) found that the variation of turbulence quantities in developed open-channel flow is very similar to that measured by Laufer (1951) in a plane channel.

the sum of the mass sources at all grid nodes arising from non-satisfaction of the continuity equation; when this had been reduced to less than half a per cent of the total mass flow through the river, iteration was stopped.

Since the governing equations are for the present problem of the elliptic type, boundary conditions must be specified for all variables around the whole flow domain. Across the channel and jet inflow boundaries the velocities and turbulence quantities were given specified values. Uniform distributions were assumed with the velocities given their experimental values, and the turbulence parameters corresponding to normal flow (see Rastogi & Rodi 1978). Along the two sides of the channel, because of the steep variations in flow properties close to the walls, a fine grid would normally be required. To avoid this, the wall-function approach as recommended by Launder & Spalding (1974) has been used. Details of this approach have been reported elsewhere (Launder & Spalding 1974; Patankar & Spalding 1970) and it suffices here to say that the existence in the near-wall region of a log-law velocity profile, and a turbulence structure which is in equilibrium is used to obtain the near-wall values of $\overline{U}$, $\overline{V}$, $\tilde{k}$ and $\tilde{\epsilon}$; for temperature, an adiabatic condition has been assumed for all walls.

At the downstream boundary of the channel flow it has been assumed that all variables have a zero x gradient. To ensure that this assumption has no significant influence on the predictions in the vicinity of the recirculation zone, it was found necessary to move the position of the downstream boundary progressively further downstream until the size of the recirculation zone became unaffected by the downstream boundary location. Usually at least one recirculation-length distance between the re-attachment point and the outflow boundary position was necessary. Similarly, the effect of the discharge on the channel flow will propagate upstream (mainly via the pressure field), leading to the curvature of the streamlines upstream of the discharge as shown in figure 1; it was essential that the inflow boundary was far enough upstream that the uniform profiles specified there (in particular the assumed zero cross-river velocities) did not contravene this fact. An analogous procedure was adopted of moving the inflow boundary location further and further upstream until the flow just in front of the discharge became unaffected.

Apart from the above checks on the influence of the boundary conditions it is also important to establish that grid-independent results have been obtained. A uniform grid was used in the y direction, but in the x direction the grid was generally only uniform across the discharge. The distance between grid lines was chosen to increase with the distance from the discharge on both sides of the jet. In this way the grid nodes could be clustered in the region of rapid variations. Once the boundary locations were established and the y grid was sufficiently fine, the grid was refined in the three main regions of the flow (upstream of the jet, in the region opposite the discharge, and in the recirculation region downstream) until enough grid points were present in each of the regions to give grid-independent results. Parameters used to judge grid independence were: jet trajectory, maximum height of separation streamline, reattachment point location, and position of vortex centre in the recirculation zone. Usually the inflow and outflow boundaries were moved once again with this final grid to ensure they were still far enough removed from the jet. A typical calculation involved 22 nodes in the y direction and 30–35 nodes in the x direction, and one example of the location of the grid lines is given in figure 1; for reasons of limited space not all the grid points in the downstream region have been included.

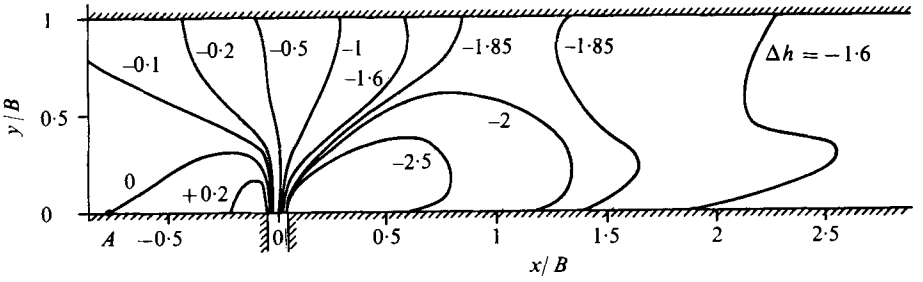

FIGURE 2. Predicted lines of constant surface elevation (for flow parameters see figure 1; Δh is relative elevation in mm above or below the water level at point A).

The storage and time requirements of the program were 40 K words and 0·00075 s/grid node/iteration/equation solved using a UNIVAC 1108 computer. A typical run in which 6 equations were solved required about 200 iterations to converge and consumed therefore approximately ten minutes of computing time.

3. Performance of the model

In this section, results are presented of the model applications to the situations studied experimentally by Mikhail *et al.* (1975), Carter (1969) and Strazisar & Prahl (1973).

3.1. *Flow pattern and surface elevation*

The streamline pattern is a useful means of illustrating the main flow features, especially in the present case of two-dimensional recirculating flows. Therefore the distribution of stream function ψ was determined from the calculated velocity field for one flow situation via the relations:

$$\frac{\partial \psi}{\partial y} = \rho \overline{U}, \quad \frac{\partial \psi}{\partial x} = -\rho \overline{V}.$$

The resulting streamline pattern and the corresponding velocity vector field are shown in figure 1; the lines of constant surface elevation for the same calculation are plotted in figure 2. The main features of the flow as illustrated by figure 1 have already been discussed in § 1; it suffices here to point out a few further details. Figure 2 shows that, owing to the blockage effect of the jet, the elevation of the channel water approaching the discharge rises at the near bank while it falls in the far-bank region. This causes the channel water to flow around the jet and to increase its velocity, as can be seen from the velocity vectors in figure 1 (*b*). The disturbance of the flow field by the discharge is still fairly strong at the final cross-section shown. The low pressure prevailing in the recirculation region which leads to the bending and reattachment of the jet can also be identified in figure 2. The maximum change in surface elevation occurs in the recirculation region and, for the situation shown in figure 2, is of the order of 3 mm. The water depth was about 5 cm in the experiment, so the use of the rigid lid approximation seems to be justified. Two streamlines deserve special attention and are therefore drawn thicker in figure 1.

The inner line is the separation streamline which constitutes the boundary of the recirculation zone and may be used to define its length L and width H_i, as shown in

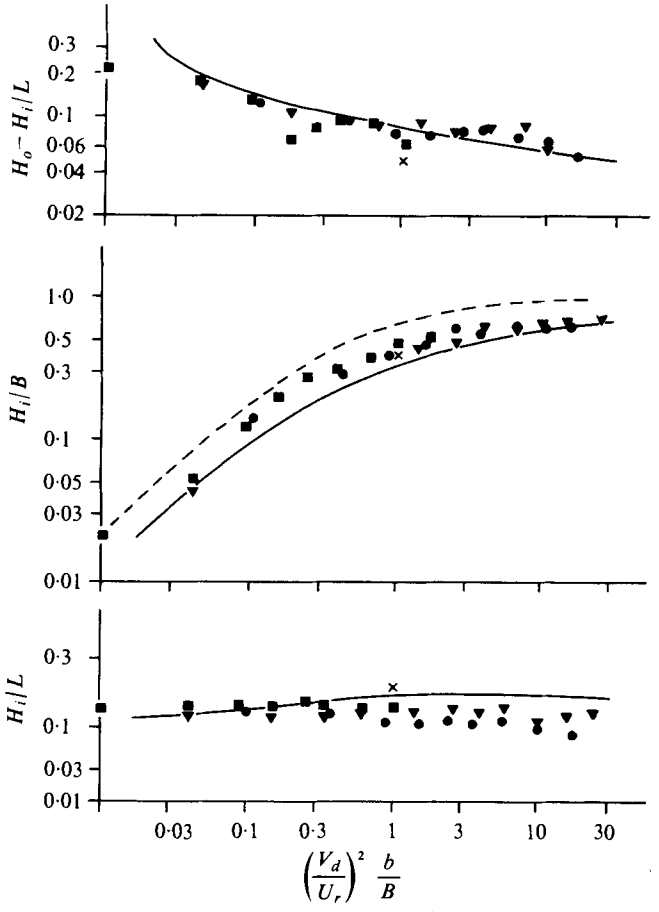

FIGURE 3. Recirculation eddy parameters. ■, b/B = 0·0105; ▼, b/B = 0·0417; ●, b/B = 0·104 (experimental data of Mikhail *et al.* 1975). ——, b/B = 0·104; ×, b/B = 0·0417 (present predictions). – – –, predictions of Mikhail *et al.* (1975).

figure 1. The outer line indicates in an approximate way (because entrainment is neglected) the outer boundary of the jet and is here used to characterize the maximum jet penetration H_0.

3.2. *Size of the recirculation region*

Figure 3 presents the variation with momentum flux ratio M of the predicted, non-dimensional width H_i/B and the width to length ratio H_i/L (the eddy shape factor) of the recirculation region, as well as the jet width $(H_0 - H_i)/L$. The measurements of Mikhail *et al.* (1975) are included for comparison.

The majority of the calculations (full line) have been carried out for a constant discharge to channel width ratio of b/B = 0·105; one calculation (cross at M = 1) was made with b/B = 0·0417 to study the influence of b/B. In accordance with the experiments, this influence is relatively small for the eddy parameters H_i/B and H_i/L (less than ten per cent change is produced); the predicted jet width $(H_0 - H_i)/L$, however, was halved by the reduction of b/B. This indicates that the latter parameter is not correlated well with the momentum flux ratio alone but depends also on b/B; this conclusion is supported by the relatively large experimental scatter for this parameter.

In the experiments, the widths H_i and H_0 were determined by injecting dye into the discharge water and then observing the inner and outer visual boundaries of the dyed jet after the dye had reached the point of maximum penetration. The observed jet boundaries can only approximately represent the two depth-averaged streamlines used to define and calculate H_i and H_0, for two reasons. First, the dye was probably not only convected by the mean motion but also diffused somewhat by the turbulent motion; second, only the dye concentration at one depth would be observed and not the depth-averaged one. Further, Mikhail *et al.* (1975) report that they had difficulty in measuring H_i accurately at small values of M. In view of these uncertainties, the agreement between predictions and experiments can be regarded as satisfactory. The shape of the recirculation eddy (characterized by H_i/L) can be seen to be nearly independent of M, while the eddy width H_i/B initially increases strongly with M but tends towards a constant value of approximately 0·7 for large values of M. This tendency is due to the interaction of the jet and channel flows combined with the relative proximity of the far bank; only a model such as the present one which can calculate the pressure field taking into consideration this influence of the far bank can predict the levelling off of the width parameter correctly. The relative jet width $(H_0 - H_i)/L$ decreases somewhat with M; this can also be interpreted as an effect of the far bank, which, for high M values, leads to a 'squeezing' of the jet between the channel flow and the recirculation bubble. Included in figure 3 is the H_i/B variation as predicted by Mikhail *et al.*'s control-volume analysis; the empirical constant was adjusted to fit the data at low values of M; this leads to noticeable overprediction for the higher M values.

The predicted reattachment length is compared with the experiments of Mikhail *et al.* and Strazisar & Prahl in figure 4. The scatter in the experimental data indicates the difficulty of measuring the location of the reattachment point, and on close examination some influence of b/B can be seen. The predictions (again for just one b/B value) tend to underestimate somewhat the eddy length over the whole range of momentum flux ratios. Finally it may be said that the underprediction of the eddy size which is obtained in the present calculations is similar in magnitude to that obtained by Pope & Whitelaw (1976), who also used a two-equation turbulence model to calculate the wake produced by the flow over a circular disk. Their conclusion that this discrepancy can be attributed to the turbulence model applies also to the present results.

3.3. *Jet trajectory and dilution*

In figure 5, predicted jet trajectories of warm water discharges are compared with Carter's (1969) measurements for three velocity ratios $R(= V_d/U_r)$. The jet trajectory is defined here as the locus of maximum jet temperature. Carter determined the trajectories by traversing thermistor probes at constant speed across the channel. This measurement technique does not yield truly time-averaged temperature values when the time scale of the turbulent motion is not small compared with the time scale of the traversing motion, which may explain the large scatter of the data. The densimetric Froude number at the discharge, $F_d = \overline{V}_d/[gh(\rho_r - \rho_d)/\rho_r]^{\frac{1}{2}}$, was quite low in Carter's experiments, ranging from 3 for $R = 2$ to 14·10 for $R = 9{\cdot}8$. Thus, there may have been some buoyancy effects in the experiments which the present model cannot account for. Such effects may have led to some stratification so that the measured temperature (presumably near the surface, but this was not stated explicitly) may not be truly

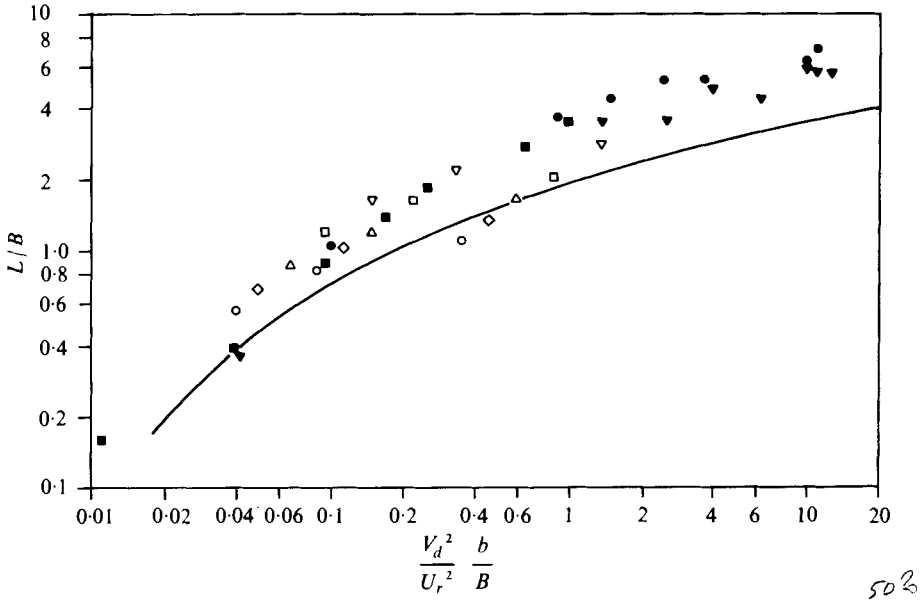

FIGURE 4. Reattachment length L. ■, $b/B = 0{\cdot}0105$; ▼, $b/B = 0{\cdot}0417$; ●, $b/B = 0{\cdot}1050$; (experimental data of Mikhail *et al.* 1975). ○, $b/B = 0{\cdot}0139$; ◇, $b/B = 0{\cdot}0182$; △, $b/B = 0{\cdot}0238$; □, $b/B = 0{\cdot}0345$; ▽, $b/B = 0{\cdot}0556$ (experimental data of Strazisar & Prahl 1973). ——, $b/B = 0{\cdot}105$ (present predictions).

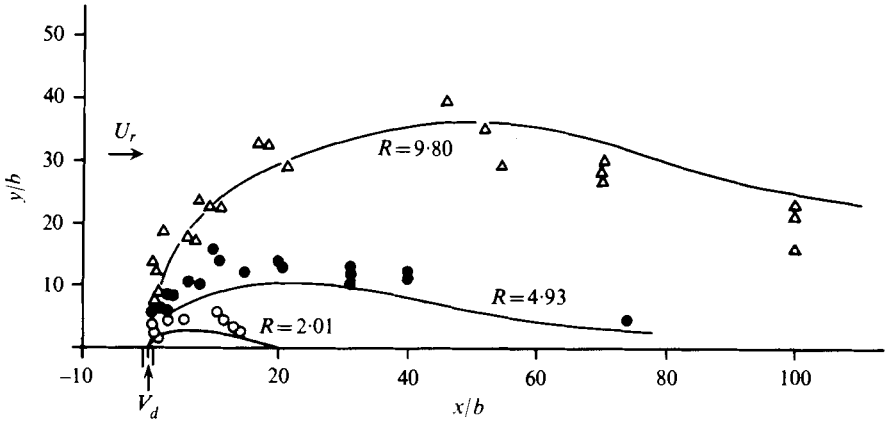

FIGURE 5. Centre-line trajectory (for symbols see figure 6).

representative of the depth-averaged temperature with which the predictions should be compared. The buoyancy effects would tend to make the warm surface layer spread further away from the discharge bank owing to buoyancy-induced pressure gradients and would be strongest at low Froude numbers. This may explain why the measured trajectories penetrate further into the channel than the predictions for the two cases with the lowest Froude number ($R = 2$ and 4·9). With these remarks in mind, the agreement between predictions and experiments appears acceptable. The model correctly predicts the increase in jet penetration with increasing velocity ratio and also the return of the maximum temperature location to the near bank.

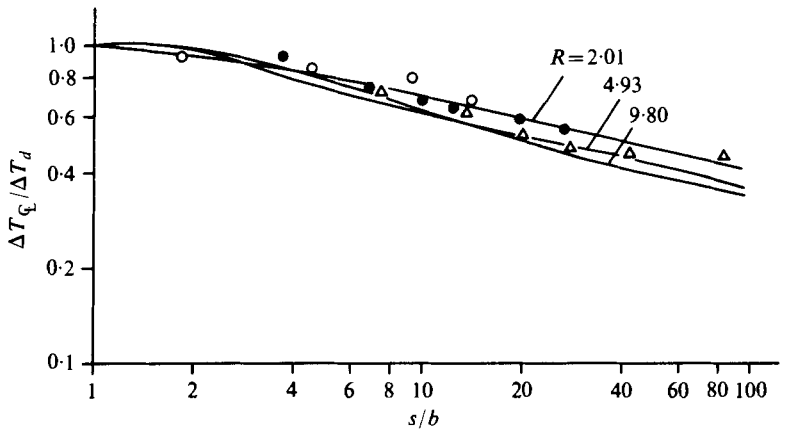

FIGURE 6. Dilution along centre-line trajectory.

Carter (1969) expts.	R	F_d
● test 11	4·93	7·1
○ test 12	2·01	3·0
△ test 13	9·80	14·1
—— predictions		

The corresponding dilution along the jet trajectory is compared in figure 6, where $\Delta T_{\mathfrak{C}}$ is the maximum temperature excess over the river temperature; the co-ordinate s is measured along the jet trajectory. Agreement is again satisfactory; the results show that the dilution is influenced very little by the velocity ratio, although the predictions indicate that the rate of dilution increases with the velocity ratio, at least in the far downstream region.

Finally, the recent experiments of Strazisar & Prahl (1973) are used to test the ability of the model to predict the effect of bottom friction on the jet trajectory; this should be represented adequately by any successful depth-averaged model. In their measurements only the ratio of jet width to jet depth $\gamma\,(=b/h)$ was changed, keeping all other parameters constant (most importantly the velocity ratio R and the channel to jet width ratio B/b). As γ decreases, the area of the jet in contact with the bottom also decreases; hence the effect of bottom friction is less, the jet loses cross-stream momentum less quickly and the jet penetration thus increases. Strazisar & Prahl used photographs of dye mixed into the discharge fluid to trace the trajectory, which they considered to be the locus of the maximum velocity. Figure 7 shows their measurements for two values of γ. Although the model predicts the higher γ value trajectory very well, the change in trajectory when γ is reduced is underpredicted. In this case it is possible that some of the discrepancy may be due to lack of knowledge concerning the exact discharge conditions, in particular the jet velocity distribution, which was probably not uniform as assumed. The pressure field shown in figure 2 indicates that the jet velocity would probably be higher toward the downstream discharge corner, and a calculation using a linear discharge velocity profile (with the same mean as before) is shown in figure 7 to illustrate the sensitivity of the calculation to this particular boundary condition. Bearing this in mind, together with the uncertainty in analysing the dye photographs, the agreement seems adequate.

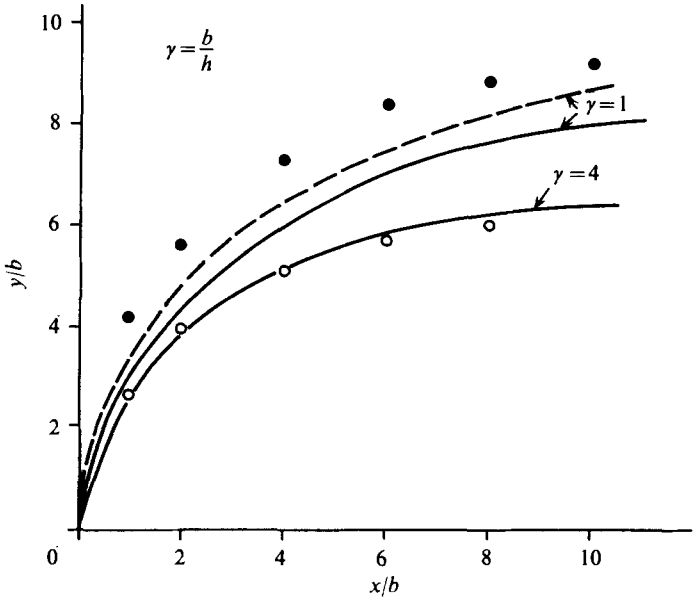

FIGURE 7. Effect of bottom friction on jet trajectory. ●, $\gamma = 1$; ○, $\gamma = 4$ (experimental data of Strazisar & Prahl 1973). ——, present predictions with $c_f = 0{\cdot}003$. – – –, with non-uniform discharge velocity.

3.4. *Isotherm pattern*

Isotherms are of particular interest to environmentalists since they show the thermally polluted river zones and also the extent to which they have been polluted. Figure 8 compares predicted depth-averaged isotherms with the measured (presumably surface) isotherms of Carter as reported by Policastro & Tokar (1972), again for the three velocity ratios for which trajectories were presented above. There is little agreement on details such as the contorted nature of the isotherms, and this is not surprising in view of the experimental uncertainties discussed above; in particular the tendency of the experimental isotherms to protrude quite far upstream of the discharge for the velocity ratio of 2 is a further indication of buoyancy effects. However, the general behaviour of the isotherms is certainly predicted correctly and also the extent of the thermally polluted regions in the streamwise and lateral directions. For the lowest velocity ratio, the heated water penetrates only 40 % of the channel width, but is carried fairly far downstream with relatively little dilution; for the highest ratio considered, however, the heated water penetrates up to 70 % of the channel and is diluted much faster; this behaviour is reproduced well by the present model.

3.5. *Considerations of local flow development to aid the estimation of numerical accuracy*

Although it was stated earlier that grid-refinement tests had confirmed the grid-independent nature of the solution, a closer look at the numerical accuracy is warranted here. The problem concerns the possible influence of numerical diffusion [see Roache (1976) for a discussion of 'numerical' or 'false' diffusion]. This occurs in all numerical solution procedures, but is a particular problem in those schemes which, like the present

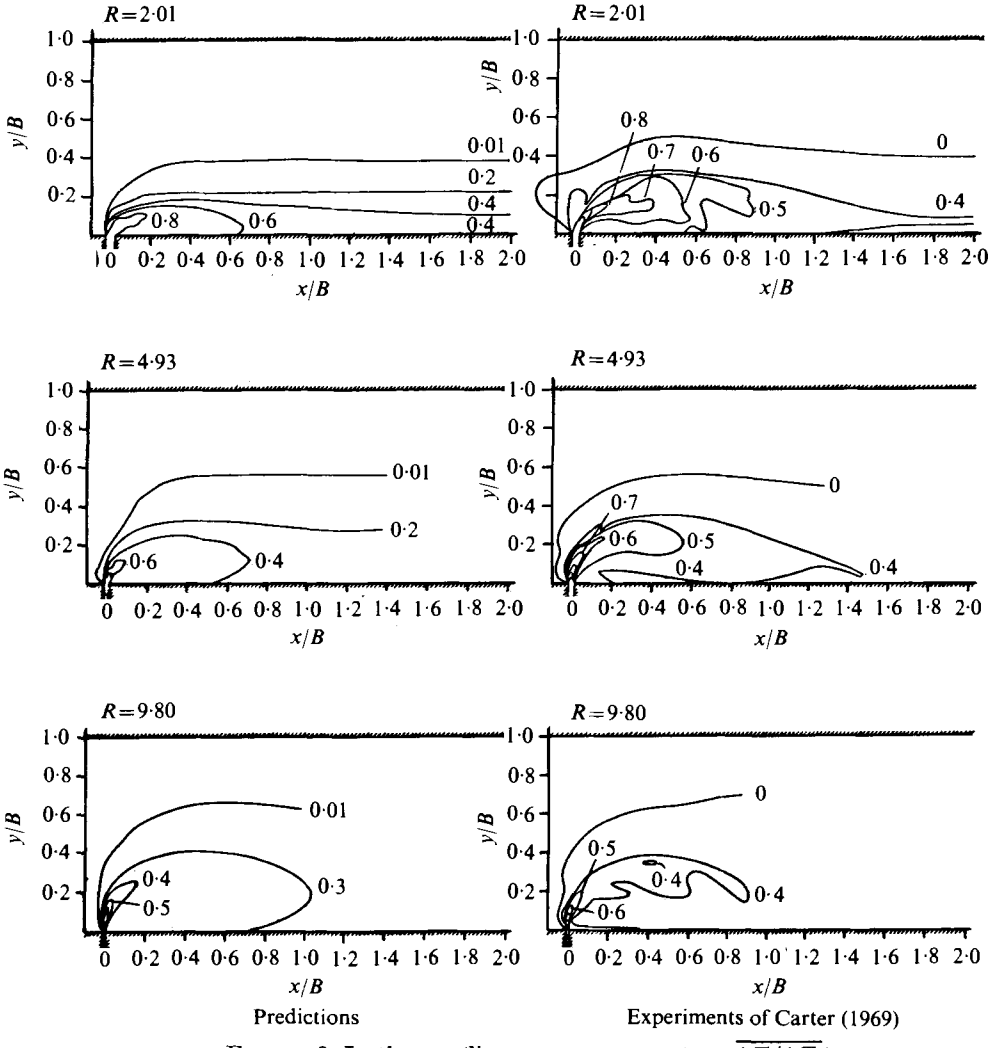

FIGURE 8. Isotherms (lines represent constant $\overline{\Delta T/\Delta T_d}$).

one, make use of the upwind-difference† approximation of the convection terms [see Gosman & Pun (1973) for details]. It has also been shown that the problem can be particularly bad when the flow is at an angle to the grid-lines (see Raithby 1976) and hence this problem deserves special attention in all recirculating flows such as the present one.

Given that the use of upwind-difference schemes introduces false diffusion, the questions then to be answered are how large is this false diffusion, and how influential is it in establishing the local values of the flow variables? In order to be able to answer these questions an examination of the processes involved in establishing the local flow development is required. Useful information is thereby gained on the differing physical processes determining the flow behaviour in different regions, and the numerical accuracy can be estimated at the same time.

† In actual fact a hybrid upwind/central difference scheme is used as recommended by Gosman & Pun (1973).

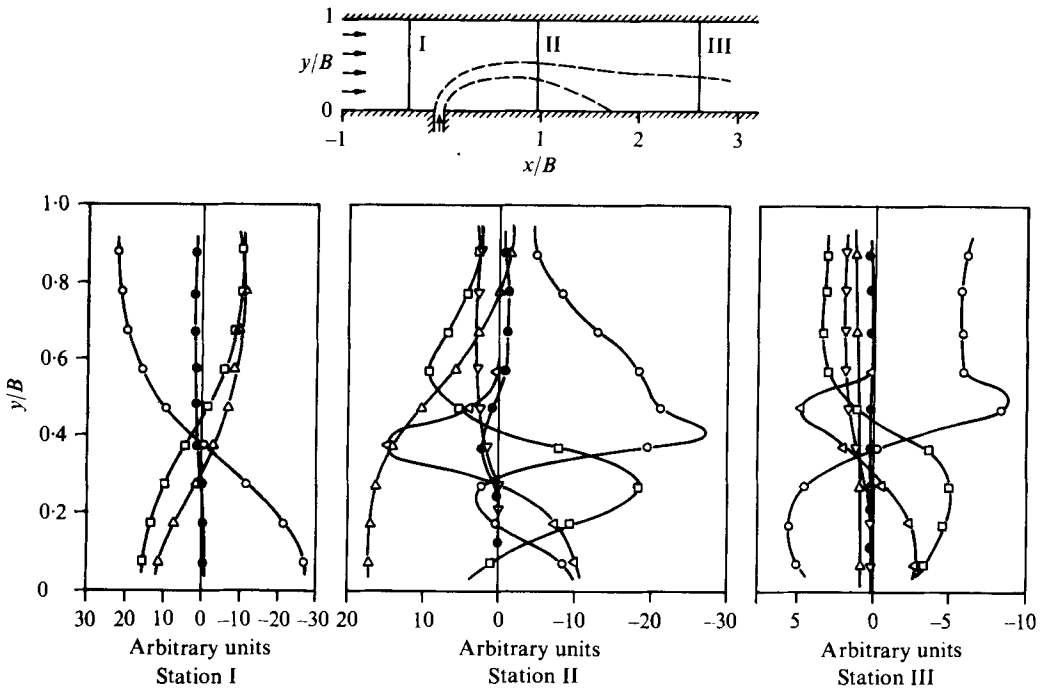

FIGURE 9. Balance of $\bar{U}$ momentum equation evaluated from numerical solution. ○, x direction convection, $\partial\bar{U}^2/\partial x$; △, pressure gradient, $+g\bar{\tau}\partial h/\partial x$; ◁, y direction diffusion, $-\partial(\bar{\tau}_{xy}/\rho)/\partial y$; □, y direction convection, $\partial\bar{U}\bar{V}/\partial y$; ▽, bottom shear, $+\tau_{bx}/\rho h$; ●, closing term (Σ all other terms).

The local flow development can be analysed in detail by examining the order of magnitude of individual terms in the momentum equations. Figure 9 shows, for three cross-sections in the channel, the balance of all terms in the $\bar{U}$ momentum equation for one calculation (for clarity only significant terms are included, e.g. x direction diffusion $\partial\bar{\tau}_{xx}/\partial x$ is too small to be plotted at all three stations). The small sketch indicates the approximate position of the three locations (i) just upstream of the discharge, (ii) just past maximum eddy height, and (iii) downstream of reattachment. These terms have been evaluated using the converged numerical solution, but central differences (i.e. second-order accurate) have been used in evaluating all terms. In obtaining the numerical solution, however, upwind differences (i.e. first-order accurate) were used at some grid-nodes for the convection terms. Thus the terms evaluated via central differences do not sum to zero; the closing term (plotted as black dots in figure 9) is an indication of the second-order truncation errors introduced into the solution owing to the use of upwind differences.

At section I (figure 9) it can be seen that there is a balance between convective terms and pressure gradient only, neither physical nor numerical diffusion playing an important role. On the near side of the channel the piling up of water in front of the discharge leads to a decelerating pressure gradient, large negative x convection and positive y convection terms which carry the channel fluid around the jet. In the far-bank region these processes are reversed in sign as the fluid accelerates to force the channel flow through a reducing area.

At sections II and III the situation is more complex, consisting of three main

regions: the outer channel flow, the recirculation zone, and an interposed shear layer. In the first region only convection, pressure gradient and bottom friction are significant; numerical diffusion is larger than physical diffusion, but small compared with the dominant terms. In the shear-layer region the numerical diffusion takes on its largest values, but there it is small compared with the turbulent diffusion. The bulge in the x convection term in the central channel region identifies the outer region of the shear layer where a slight velocity excess is still present. The change in sign of the diffusion term shows that the shear layer is losing momentum by diffusion into the recirculation region. In the final section (III) the pressure gradient is uniform over the whole channel and is relatively small, indicating that the flow is becoming more boundary-layer like (the elliptic effects in the differential equation are disappearing). The shear-layer region extends now past the centre-line of the channel but is considerably weaker (note the change of scale from sections I to II to III); momentum is still being lost by the faster moving fluid and transferred by diffusion into the wake-like flow behind the recirculation eddy. Once more the closure terms indicate that numerical diffusion at this section is of no significance.

The above discussion now reinforces the claim for grid-independence of the results and was further confirmed by using the formula of de Vahl Davis & Mallinson (1972)† to evaluate the false diffusion coefficient. This was less than the turbulent viscosity (but always considerably larger than the laminar viscosity) at all stations other than just before or just after the discharge; here, however, an examination of the $\bar{U}$ momentum equation indicated that the flow was characterized by the convection/pressure balance shown at station I in figure 9. The dangers of merely examining ν_{num} however are well illustrated by this example.

3.6. *Model input sensitivity tests*

A few additional computations were carried out in order to examine the sensitivity of the predictions to the assumptions made in the mathematical model of § 2. The details and results are summarized in table 2. The various runs listed in the table were carried out for the same flow situation, using the same numerical grid. Because the recirculation eddy is the main feature of the flow considered here, the predicted eddy parameters were chosen as the basis for the sensitivity analysis. Run 1 serves as reference a calculation; it was obtained with the model and the empirical constants described in § 2, and its results have been discussed in § 3.2.

In runs 2 and 3, the bottom-friction coefficient c_f was respectively half and double its original value of 0·003. This change in c_f can be seen to cause less than 5 % change in the recirculation eddy parameters. The relatively small sensitivity of the predictions to the friction coefficient c_f is comforting since c_f is not normally known with great accuracy for a particular channel. In the present case, however, the insensitivity is, as can be seen from figure 9, due to the fact that flow in smooth laboratory channels has been considered, in which bottom friction does not always play a dominating role. The direction of the small change in the results is as expected: when the bottom shear

† $$\nu_{num} = \frac{V\Delta x\,\Delta y\,|\sin 2\alpha|}{4(\Delta y\,|\sin\alpha|^3 + \Delta x\,|\cos\alpha|^3)}.$$

ν_{num} is the false diffusion coefficient, V the magnitude of the local velocity vector, α its angle to the x axis and Δx and Δy are the local grid spacings.

Run	Details	$\frac{H_i}{B}$	$\frac{L}{B}$	$\frac{H_i}{L}$	$\frac{H_0-H_i}{L}$
1	$M = 1, R = 3{\cdot}16, b/B = 0{\cdot}105$ Model of § 2	0·33	1·8	0·18	0·095
2	as 1 but $c_f = \frac{1}{2}c_f$	0·34	1·9	0·175	0·094
3	as 1 but $c_f = 2c_f$	0·324	1·71	0·19	0·10
4	as 1 but $\nu_t = 0$	0·43	3·0	0·14	0·051
5	as 1 but $\nu_t = \nu$	0·43	3·0	0·14	0·050

TABLE 2. Model input sensitivity tests.

is reduced, both the width and the length of the recirculation eddy increase. This is in agreement with Strazisar & Prahl's (1973) experimental observation that the jet penetration increases with increasing h/b, in which case the bottom shear becomes less important; this influence of the bottom friction has already been examined in figure 7.

Runs 4 and 5 were carried out to examine the influence of both physical and numerical diffusion of momentum. In run 4 physical diffusion was put to zero ($\tilde{\nu}_t = 0$) and in run 5 it was kept small by replacing the turbulent viscosity $\tilde{\nu}_t$ by the laminar viscosity ν. The results of the two runs are nearly identical. As shown by Flokstra (1976), a recirculation region can be generated in a steady-flow depth-averaged calculation only when diffusion is present (even unintentionally). The results of runs 4 and 5 indicate therefore that the numerical diffusion, for the grid used, was much larger than the laminar diffusion, confirming the results of calculations mentioned in § 3.5. The considerations of § 3.5 have also shown that numerical diffusion is significantly smaller than turbulent diffusion in those regions where diffusion is important. This explains why the predictions of run 1 (which includes turbulent diffusion) are markedly different from those of runs 4 and 5.

In the reference run 1, the turbulent viscosity $\tilde{\nu}_t$ determined from the $\tilde{k}, \tilde{\varepsilon}$ model was 20 to 1000 times larger than the laminar viscosity ν, depending on the position in the flow. In order to test the sensitivity of the predictions to a varying turbulent viscosity, a few runs were carried out in which a uniform $\tilde{\nu}_t$ over the whole flow domain was used at a value 200 times the laminar viscosity ν. For the conditions of run 1, this produced eddy parameters very similar to those obtained with the $\tilde{k}, \tilde{\varepsilon}$ model. For other momentum flux ratios however, this value of $\tilde{\nu}_t$ gave very poor agreement with the experimental eddy parameters. This indicates that constant turbulent viscosity is too crude an assumption to use in a general model for the near field of side discharges, and a refined turbulence model as used in the present paper is required.

4. Conclusions

A two-dimensional calculation method for open-channel flows with recirculation zones has been described which combines depth-averaged forms of the governing equations with an advanced turbulence model. The application of the method to the practically important heated side discharge problem has shown that the velocity and temperature behaviour can be predicted correctly for this problem. In particular, the method describes well the influence of the momentum flux ratio M (or the velocity ratio

R when the far-bank influence is small) on the size and shape of the recirculation zone and on the temperature distribution in the channel. This success indicates that the assumptions on which the mathematical model is based are realistic, viz. the turbulence-model assumptions, the neglect of dispersion terms, and the rigid lid approximation. By considering the individual terms in the $\overline{U}$ momentum equation, the influence of numerical diffusion was examined and found to be small; the numerical accuracy of the predictions was therefore shown to be acceptable. It should be emphasized that the turbulence-model constants were not tuned to suit the present problem but were simply taken from the literature, where they were determined by reference to entirely different flow situations, none of which possessed recirculating regions. Compared with the use of a constant turbulent viscosity as adopted in most existing calculation methods for open-channel flow, the $\tilde{k}$, $\tilde{\epsilon}$ turbulence model was found to offer much greater generality.

The main limitation of the mathematical model is its restriction to two-dimensional flows. Thus, the model cannot account for stratification or secondary currents in the cross-sectional plane of the river caused by buoyancy, river curvature or other effects. The limits of applicability have yet to be determined by further testing; also more comparisons are required with velocity and surface-elevation data, but unfortunately such data are very scarce for the present flow.

The application of the model should be restricted to the relatively short river stretches with recirculation regions; for stretches without recirculation the boundary-layer-type model of Rastogi & Rodi (1978) is better suited because it is more economical and can handle gradually varied flow. The model as described is, however, not restricted to the right-angle discharge problem considered here; angled discharges and intake/discharge situations for example can be calculated without difficulty. Indeed, the model has already been successfully applied to the intake/discharge problem (see Fink 1977). Many problems of practical relevance are therefore within the scope of the present model. Verification against laboratory data is of course only the first test of any proposed model: the results presented herein however indicate that the present model has performed sufficiently well in this test that it can, and should, now be applied to a real-life discharge problem.

The computations described in the present paper were carried out on the UNIVAC 1108 computer of the University of Karlsruhe.

REFERENCES

Carter, H. H. 1969 A preliminary report on the characteristics of a heated jet discharged horizontally into a transverse current. Part 1 – constant depth. *Chesapeake Bay Inst., Johns Hopkins Univ. Tech. Rep.* no. 61.

De Vahl Davis, G. & Mallinson, G. D. 1972 False diffusion in numerical fluid mechanics. *School Mech. Indust. Engng, Univ. New South Wales Rep.* no. 1972/FMT/1.

Fink, L. 1977 Abschätzung der Rezirkulationsgefahr bei Brauchwasser-Entnahme- und Rückgabesystemen in Fließgewässern. *Wasserwirtschaft* **67** (3), 65–70.

Fischer, H. 1973 Longitudinal dispersion and transverse mixing in open-channel flow. *Ann. Rev. Fluid Mech.* **5**, 59–78.

Flokstra, C. 1976 Generation of two-dimensional horizontal secondary currents. *Delft Hydraul. Lab. Res. Rep.* S 163, part II.

GOSMAN, A. D. & PUN, W. M. 1973 Lecture notes for course entitled – Calculation of recirculating flows. *Heat Transfer Section, Dept. Mech. Engng, Imp. Coll. Rep.* HTS/74/2.

JIRKA, G. H., ABRAHAM, G. & HARLEMAN, D. R. F. 1975 An assessment of techniques for hydrothermal prediction. *Final Rep. to U.S. Atomic Energy Comm., R. M. Parsons Lab. Water Resources Hydrodyn., Dept. Civil Engng, MIT Rep.* no. 203.

KUIPERS, J. & VREUGDENHIL, C. B. 1973 Calculations of two-dimensional horizontal flow. *Delft Hydraul. Lab. Rep.* S 163, part 1.

LAUFER, J. 1951 Investigation of turbulent flow in a two-dimensional channel. *N.A.C.A. Rep.* no. 1053.

LAUNDER, B. E., MORSE, A., RODI, W. & SPALDING, D. B. 1972 Prediction of free shear flows – a comparison of the performance of six turbulence models. *Proc. Conf. Free Turbulent Shear Flows, N.A.S.A. Langley Research Center*, vol. 1, pp. 361–422.

LAUNDER, B. E. & SPALDING, D. B. 1974 The numerical computation of turbulent flows. *Comp. Meth. in Appl. Mech. Engng* **3**, 269–289.

LEENDERTSE, J. J. 1967 Aspects of a computational model for long period water wave propagation. *Rand Corp. Mem.* RM-5294-PR.

LOZIUK, L. A., ANDERSON, J. C. & BELYTSCHKO, E. 1972 Hydrothermal analysis by finite-element method. *J. Hydraul. Div., Proc. A.S.C.E.* **98** (HY3), 1983–1997.

MIKHAIL, R., CHU, V. H. & SAVAGE, S. B. 1975 The reattachment of a two-dimensional turbulent jet in a confined cross flow. *Proc. 16th IAHR Cong., São Paulo, Brazil*, vol. 3, pp. 414–419.

NAKAGAWA, H., NEZU, I. & UEDA, H. 1975 Turbulence of open-channel flow over smooth and rough beds. *Proc. Japan Soc. Mech. Engrs* **241**, 155–168.

PATANKAR, S. V. & SPALDING, D. B. 1970 *Heat and Mass Transfer in Boundary Layers*, 2nd edn. London: Intertext Books.

PATANKAR, S. V. & SPALDING, D. B. 1972 A calculation procedure for heat, mass and momentum transfer in three-dimensional parabolic flows. *Int. J. Heat Mass Transfer* **15**, 1787–1806.

POLICASTRO, A. J. & TOKAR, J. V. 1972 Heated effluent dispersion in large lakes – state of the art of analytical modelling. Part I: critique of model formulations. *Argonne Nat. Lab. Centre for Environmental Studies Rep.* ANL/ES-11.

POPE, S. B. & WHITELAW, J. H. W. 1976 The calculation of near-wake flows. *J. Fluid Mech.* **73**, 9–32.

RAITHBY, G. 1976 Skew upstream differencing schemes for problems involving fluid flow. *Comp. Meth. in Appl. Mech. Engng* **9**, 151–162.

RASTOGI, A. K. & RODI, W. 1978 Two- and three-dimensional calculations of heat and mass transfer in open channel flows. *J. Hydraul. Div., Proc. A.S.C.E.* (in press).

ROACHE, P. J. 1976 *Computational Fluid Mechanics*. Hermosa Publishers.

ROUSE, H. 1957 Diffusion in the lee of a two-dimensional jet. *Proc. 9th Cong. Int. Méc. Appl., Univ. Bruxelles.*

SPALDING, D. B. 1975 THIRBLE – Transfer of heat in rivers, bays, lakes and estuaries. *Heat Transfer Section, Dept. Mech. Engng, Imp. Coll. Rep.* HTS/75/4.

STRAZISAR, A. & PRAHL, J. 1973 The effects of bottom friction on river entrance flow with crossflow. *Proc. 16th Conf. Great Lakes Res.* pp. 615–625.